DOI: 10.1021/ic102420x

Inorganic Chemistry
Article

Combining NMR of Dynamic and Paramagnetic Molecules: Fluxional High-Spin Nickel(II) Complexes Bearing Bisguanidine Ligands†

Pascal Roquette, Astrid Maronna, Matthias Reinmuth, Elisabeth Kaifer, Markus Enders,* and Hans-Jörg Himmel*

Contribution from the Department of Inorganic Chemistry, Ruprecht-Karls-Universität Heidelberg, Im Neuenheimer Feld 270, 69120 Heidelberg, Germany

Received December 3, 2010

A detailed nuclear magnetic resonance (NMR) study was carried out on a series of paramagnetic, tetrahedrally coordinated nickel(II) dihalide complexes featuring chelating guanidine ligands. A complete assignment of the NMR signals for all complexes was achieved by sophisticated NMR experiments, including correlation spectra. The effects of halide exchange, as well as the variation in the guanidine−metal bite angles on the paramagnetic shifts, were assessed. The paramagnetic shift was derived with the aid of the diamagnetic NMR spectra of the analogous Zn complexes, which were synthesized for this purpose. The experimentally derived paramagnetic shift was then compared with the values obtained from quantum chemical (DFT) calculations. Furthermore, variable-temperature NMR studies were recorded for all complexes. It is demonstrated that NMR spectroscopy can be applied to evaluate the rate constants of fast fluxional processes within paramagnetic and catalytically active metal complexes.

1. Introduction

Since the development of transition-metal complexes as powerful homogeneous catalysts in numerous reactions, there is a growing demand for potent tools to analyze the conformational structure and dynamics of active species in solution during reaction. For diamagnetic compounds, nuclear magnetic resonance (NMR) techniques generally allow determination of the three-dimensional (3D) structure and analysis of the fluxional processes in solution. Many catalysts, involving heavier transition metals, are diamagnetic and permit the use of an arsenal of modern NMR techniques. However, the common paramagnetism of related compounds of less-expensive metals of the first transition row, which become increasingly important for catalysis,[1] often hinders NMR analysis.

Paramagnetic substances may lead to NMR spectra over a large chemical shift range with considerable signal broadening. Signal assignment is difficult and the fast relaxation hampers the use of complex pulse sequences (e.g., most two-dimensional (2D) techniques). Although many researchers limit the use of NMR spectroscopy to diamagnetic substances, in the last decades, advances in theory, computer performance, and NMR instrumentation have made it possible to analyze paramagnetic complexes by NMR in more detail. For these experiments, the electron−nucleus interaction must be taken into account. Until now, a variety of metal complexes of

† Dedicated to Professor Hansgeorg Schnöckel on the occasion of his 70th birthday.

*Authors to whom correspondence should be addressed. E-mail: markus.enders@uni-hd.de (M.F.), hans-jorg.himmel@aci.uni-heidelberg.de (H.J.H.).

(1) Recent examples for paramagnetic molecular catalysts include: (a) Katsuki, T. *Coord. Chem. Rev.* **1995**, *140*, 189–214. (b) Theopold, K. H. *Eur. J. Inorg. Chem.* **1998**, 15–24. (c) Canali, L.; Sherrington, D. C. *Chem. Soc. Rev.* **1999**, *28*, 85–93. (d) Britovsek, G. J. P.; Bruce, M.; Gibson, V. C.; Kimberley, B. S.; Maddox, P. J.; Mastroianni, S.; McTavish, S. J.; Redshaw, C.; Solan, G. A.; Strömberg, S.; White, A. J. P.; Williams, D. J. *J. Am. Chem. Soc.* **1999**, 8728–8740. (e) Fürstner, A. *Chem. Rev.* **1999**, *99*, 991–1046. (f) Döhring, A.; Göhre, J.; Jolly, P. W.; Kryger, B.; Rust, J.; Verhovnik, G. P. J. *Organometallics* **2000**, *19*, 388–402. (g) Gambarotta, S. *Coord. Chem. Rev.* **2003**, *237*, 229–243. (h) Bolm, C.; Legros, J.; Le Paih, J.; Zani, L. *Chem. Rev.* **2004**, *104*, 6217–6254. (i) Gromada, J.; Carpentier, J.-F.; Mortreux, A. *Coord. Chem. Rev.* **2004**, *238*, 397–410. (j) Jones, D. J.; Gibson, V. C.; Green, S. M.; Maddox, P. J.; White, A. J. P.; Williams, D. J. *J. Am. Chem. Soc.* **2005**, *127*, 11037–11046. (k) Wass, D. F. *Dalton Trans.* **2007**, 816–819. (l) Sherry, B. D.; Fürstner, A. *Acc. Chem. Res.* **2008**, *41*, 1500–1511. (m) *Iron Catalysis in Organic Chemistry: Reactions and Applications*; Plietker, B., Ed.; Wiley−VCH Verlag GmbH & Co. KGaA: Weinheim, Germany, 2008; p xvi + 280 pp. (n) Kirillov, E.; Roisnel, T.; Razavi, A.; Carpentier, J.-F. *Organometallics* **2009**, *28*, 2401–2409. (o) Coeffard, V.; Aylward, M.; Guiry, P. J. *Angew. Chem., Int. Ed.* **2009**, *48*, 9152–9155. (p) Kaminsky, W.; Funck, A.; Hähnsen, H. *Dalton Trans.* **2009**, *41*, 8803–8810. (q) Khamker, Q.; Champouret, Y. D. M.; Singh, K.; Solan, G. A. *Dalton Trans.* **2009**, *41*, 8935–8944. (r) Organo, V. G.; Filatov, A. S.; Quartararo, J. S.; Friedman, Z. M.; Rybak-Akimova, E. V. *Inorg. Chem.* **2009**, *48*, 8456–8468. (s) England, J.; Gondhia, R.; Bigorra-Lopez, L.; Petersen, A. R.; White, A. J. P.; Britovsek, G. J. P. *Dalton Trans.* **2009**, *27*, 5319–5334. (t) Kemper, S.; Hrobarik, P.; Kaupp, M.; Schloerer, N. E. *J. Am. Chem. Soc.* **2009**, *131*, 4172–4173. (u) Albahily, K.; Al-Baldawi, D.; Gambarotta, S.; Duchateau, R.; Koc, E.; Burchell, T. J. *Organometallics* **2008**, *27*, C.5708–5711. (v) Comba, P.; Lang, C.; Lopez de Laorden, C.; Muruganantham, A.; Rajaraman, G.; Wadepohl, H.; Zajaczkowski, M. *Chem.—Eur. J.* **2008**, *14*, 5313–5328. (w) Russell, S.; Darmon, J.; Lobkovsky, E.; Chirik, P. *Inorg. Chem.* **2010**, *49*, 2782.

(2) Review articles about paramagnetic NMR spectroscopy include: (a) Bertini, I.; Luccinat, C. NMR of Paramagnetic Substances. *Coord. Chem. Rev.* **1996**, *150*, 1−296. (b) Köhler, F. H. In *Magnetism: Molecules to Materials*; Miller, J. S., Drillon, M., Eds.; Wiley−VCH: Weinheim, Germany, 2001; pp 379−430. (c) Bertini, I.; Luchinat, C.; Parigi, G. *Prog. Nucl. Magn. Reson. Spectrosc.* **2002**, *40*, 249–273. (d) Bertini, I.; Luchinat, C.; Parigi, G.; Pierattelli, R. *ChemBioChem* **2005**, *6*, 1536–1549. (e) Rastrelli, F.; Bagno, A. *Chem.—Eur. J.* **2009**, 7990–8004. (f) Kaupp, M.; Köhler, F. H. *Coord. Chem. Rev.* **2009**, *253*, 2376–2386.

Published on Web 01/26/2011

paramagnetic first-row transition metals have been characterized by NMR spectroscopy.[2−17] The method became important in the characterization of complexes of metals such as cobalt and iron (e.g., in metalloporphyrins[7] or Rubredoxin[8]), as well as nickel(II).[9] One should particularly mention the extensive research on paramagnetic hemes and heme proteins, as well as metalloporphyrins carried out by LaMar et al. and by Walker et al.[10,11] In the field of 4-fold-coordinated nickel(II) complexes, several NMR investigations have been performed already during the 1960s, especially those by Benson et al. and Holm et al.[12−17]

Guanidines and guanidinates are well-established as versatile ligand systems.[18−25] We are interested in the properties of nickel(II) complexes bearing strong σ-donor guanidino groups bridged by aromatic units of different size, which are potential precatalysts (e.g., in olefin polymerization reactions). We recently reported the syntheses of some new nickel(II)halide complexes featuring the bisguanidines btmgb

(3) (a) Hebendanz, N.; Köhler, F. H.; Scherbaum, F.; Schlesinger, B. *Magn. Reson. Chem.* **1989**, *27*(8), 798–802. (b) Köhler, F. H.; Metz, B.; Strauss, W. *Inorg. Chem.* **1995**, *34*(17), 4402–4413. (c) Bräunlein, B.; Köhler, F. H.; Strauss, W.; Zeh, H. *Z. Naturforsch. B: Chem. Sci.* **1995**, *50*(11), 1739–1747. (d) Feher, R.; Köhler, F. H.; Nief, F.; Ricard, L.; Rossmayer, S. *Organometallics* **1997**, *16*, 4606–4610. (e) Gattinger, I.; Herker, M. A.; Hiller, W.; Köhler, F. H. *Inorg. Chem.* **1999**, *38*(10), 2359–2368. (f) Heigl, O. M.; Herdtweck, E.; Grasser, S.; Köhler, F. H.; Strauss, W.; Zeh, H. *Organometallics* **2002**, *21*(17), 3572–3579. (g) Köhler, F. H.; Mölle, R.; Strauss, W.; Weber, B.; Gedridge, R. W.; Basta, R.; Trakarnpruk, W.; Tomaszewski, R.; Arif, A. M.; Ernst, R. D. *Organometallics* **2003**, *22*(9), 1923–1930.

(4) Knorr, R.; Hauer, H.; Weiss, A.; Polzer, H.; Ruf, F.; Löw, P.; Dvortsák, P.; Böhrer, P. *Inorg. Chem.* **2007**, *46*, 8379–8390.

(5) Fernández, P.; Pritzkow, H.; Carbó, J.; Hofmann, P.; Enders, M. *Organometallics* **2007**, *26*, 4402–4412.

(6) Schmedt auf der Günne, J. *Angew. Chem., Int. Ed.* **2009**, *48*, 3401–3403.

(7) Mao, J.; Zhang, Y.; Oldfield, E. *J. Am. Chem. Soc.* **2002**, *124*, 13911–13920.

(8) Wilkens, S. J.; Xia, B.; Weinhold, F.; Markley, J. L.; Westler, W. M. *J. Am. Chem. Soc.* **1998**, *120*, 4806–4814.

(9) Belle, C.; Bougault, C.; Averbuch, M.-T.; Durif, A.; Pierre, J.-L.; Latour, J.-M.; Le Pape, L. *J. Am. Chem. Soc.* **2001**, *123*, 8053–8066.

(10) (a) La Mar, G. N.; Walker, F. A. NMR Studies of Paramagnetic Metalloporphyrins. In *The Porphyrins*, Vol. *IV*; Dolphin, D., Ed.; Academic Press: New York, 1979; pp 61−157. (b) Walker, F. A.; Simonis, U. Proton NMR Spectroscopy of Model Hemes. In *Biological Magnetic Resonance*, Vol. *12*: NMR of Paramagnetic Molecules; Berliner, L. J., Reuben, J., Eds.; Plenum Press: New York, 1993; pp 133−274. (c) Walker, F. A. *Coord. Chem. Revs.* **1999**, *185−186*, 471–534. (d) Walker, F. A. Proton NMR and EPR Spectroscopy of Paramagnetic Metalloporphyrins. In *The Porphyrin Handbook*; Kadish, K. M., Smith, K. M., Guilard, R., Eds.; Academic Press: Boston; 2000, Vol. *5*; pp 81−183. (e) La Mar, G. N.; Satterlee, J. D.; De Ropp, J. S.Nuclear magnetic resonance of hemoproteins. In *The Porphyrin Handbook*; Kadish, K. M., Smith, K. M., Guilard, R., Eds.; Academic Press: Boston; 2000, Vol. *5*; pp 185−298. (f) Walker, F. A. *Inorg. Chem.* **2003**, *42*, 4526–4544. (g) Walker, F. A.; Licoccia, S.; Paolesse, R. *J. Inorg. Biochem.* **2006**, *100*, 810–837.

(11) See, for examples of dynamic studies: (a) Pignolet, L. H.; Lewis, R. A.; Holm, R. H. *Inorg. Chem.* **1972**, *11*, 99–104. (b) La Mar, G. N.; Walker, F. A. *J. Am. Chem. Soc.* **1972**, *94*, 8607–8608. (c) Shokhirev, N. V.; Shokhireva, T. Kh.; Polam, J. R.; Watson, C. T.; Raffii, K.; Simonis, U.; Walker, F. A. *J. Phys. Chem. A* **1997**, *101*, 2778–2886. (d) Walker, F. A. *Inorg. Chem.* **1999**, *38*, 5856–5859. (e) Yatsunyk, L. A.; Walker, F. A. *Inorg. Chem.* **2004**, *43*, 757–777. (f) Yatsunyk, L. A.; Ogura, H.; Walker, F. A. *Inorg. Chem.* **2005**, *44*, 2867–2881.

(12) Phillips, W. D.; Benson, R. E. *J. Chem. Phys.* **1960**, *33*, 607–608.

(13) Benson, R. E.; Eaton, D. R.; Josey, A. D.; Phillips, W. D. *J. Am. Chem. Soc.* **1961**, *83*, 3714–3716.

(14) Eaton, D. R.; Josey, A. D.; Benson, R. E.; Phillips, W. D.; Cairns, T. L. *J. Am. Chem. Soc.* **1962**, *84*, 4100–4106.

(15) Eaton, D. R.; Josey, A. D.; Phillips, W. D.; Benson, R. E. *Mol. Phys.* **1962**, *5*, 407–416.

(16) Eaton, D. R.; Josey, A. D.; Phillips, W. D.; Benson, R. E. *J. Chem. Phys.* **1962**, *37*, 347–360.

(17) (a) Parks, J. E.; Holm, R. H. *Inorg. Chem.* **1968**, *7*, 1408–1416. (b) Ernst, R. E.; O'Connor, M. J.; Holm, R. H. *J. Am. Chem. Soc.* **1968**, *90*, 5305–5306. (c) Ernst, R. E.; O'Connor, M. J.; Holm, R. H. *J. Am. Chem. Soc.* **1968**, *90*, 5735–5744.

(18) (a) Edelmann, F. T. *Adv. Organomet. Chem.* **2008**, *57*, 183–352. (b) Edelmann, F. T. *Chem. Soc. Rev.* **2009**, *38*, 2253–2268.

(19) (a) Coles, M. P. *Dalton Trans.* **2006**, 985–1001. (b) Coles, M. P. *Chem. Commun.* **2009**, 3659–3676. (c) Coles, M. P.; Aragón-Sáez, P. J.; Oakley, S. H.; Hitchcock, P. B.; Davidson, M. G.; Maksić, Z. B.; Vianello, R.; Leito, I.; Kaljurand, I.; Apperley, D. C. *J. Am. Chem. Soc.* **2009**, *131*, 16858–16868.

(20) (a) Cotton, F. A.; Matonic, J. H.; Murillo, C. A. *J. Am. Chem. Soc.* **1997**, *19*, 7889–7890. (b) Cotton, F. A.; Daniels, L. M.; Murillo, C. A.; Timmons, D. J. *J. Chem. Soc., Chem. Commun.* **1997**, 1449–1450. (c) Cotton, F. A.; Gruhn, N. E.; Gu, J.; Huang, P.; Lichtenberger, D. L.; Murillo, C. A.; Van Dorn, L. O.; Wilkinson, C. C. *Science* **2002**, *298*, 1971–1974. (d) Cotton, F. A.; Gu, J.; Murillo, C. A.; Timmons, D. J. *J. Am. Chem. Soc.* **1998**, *120*, 13280–13281. (e) Cotton, F. A.; Donahue, J. P.; Lichtenberger, D. L.; Murillo, C. A.; Villagrán, D. *J. Am. Chem. Soc.* **2005**, *127*, 10808–10809. Cotton, F. A.; Dalal, N. S.; Huang, P.; Ibragimov, S. A.; Murillo, C. A.; Piccoli, P. M. B.; Ramsey, C. M.; Schultz, A. J.; Wang, X.; Zhao, Q. *Inorg. Chem.* **2007**, *46*, 1718–1726.

(21) (a) Würtele, C.; Gaoutchenova, E.; Harms, K.; Holthausen, M. C.; Sundermeyer, J.; Schindler, S. *Angew. Chem., Int. Ed.* **2006**, *45*, 3867–3869. (b) Maiti, D.; Lee, D.-H.; Gaoutchenova, K.; Würtele, C.; Hothausen, M. C.; Sarjeant, A. A. N.; Sundermeyer, J.; Schindler, S.; Karlin, K. D. *Angew. Chem., Int. Ed.* **2007**, *47*, 82–85. (c) Lanci, M. P.; Smirnov, V. V.; Cramer, C. J.; Gauchenova, E. V.; Sundermeyer, J.; Roth, J. P. *J. Am. Chem. Soc.* **2007**, *129*, 14697–14709. (d) Maiti, D.; Lee, K.; Gaoutchenova, D.-H.; Würtele, C.; Holthausen, M. C.; Sarjeant, A. A. N.; Sundermeyer, J.; Schindler, S.; Karlin, K. D. *Angew. Chem., Int. Ed.* **2008**, *47*, 82–85.

(22) Herres-Pawlis, S. *Nachr. Chem.* **2009**, *57*, 20–23.

(23) (a) Pohl, S.; Harmjanz, M.; Schneider, J.; Saak, W.; Henkel, G. *J. Chem. Soc., Dalton Trans.* **2000**, 3473–3479. (b) Petrovic, D.; Hill, L. M. R.; Jones, P. G.; Tolman, W. B.; Tamm, M. *Dalton Trans.* **2008**, 887–894. (c) Filimon, S.-A.; Hrib, C. G.; Randoll, S.; Neda, I.; Jones, P. G.; Tamm, M. *Z. Anorg. Allg. Chem.* **2010**, *636*, 691–699.

(24) (a) Carmalt, C. J.; Newport, A. C.; O'Neill, S. A.; Parkin, I. P.; White, A. J. P.; Williams, D. J. *Inorg. Chem.* **2005**, *44*, 615–619. (b) Rische, D.; Parala, H.; Gemel, H. E.; Winter, M.; Fischer, R. A. *Chem. Mater.* **2006**, *18*, 6075–6082. (c) Milanov, A. P.; Bhakta, R.; Baunemann, A.; Becker, H.-W.; Thomas, R.; Ehrhart, P.; Winter, M.; Devi, A. *Inorg. Chem.* **2006**, *45*, 11008–11018. (d) Coyle, J. P.; Monillas, W. H.; Yap, G. P. A.; Barry, S. T. *Inorg. Chem.* **2008**, *47*, 683–689. (e) Coyle, J. P.; Monillas, W. H.; Yap, G. P. A.; Barry, S. T. *Inorg. Chem.* **2008**, *47*, 683–689. (f) Baunemann, A.; Bekermann, D.; Thiede, T. B.; Parala, H.; Winter, M.; Gemel, C.; Fischer, R. A. *Dalton Trans.* **2008**, *28*, 3715–3722. (g) Milanov, A. P.; Thiede, T. B.; Devi, A.; Fischer, R. A. *J. Am. Chem. Soc.* **2009**, *131*, 17062–17063. (h) Potts, R. A.; Carmalt, C. J.; Blackman, C. S.; Abou-Chahine, F.; Pugh, D.; Davies, H. O. *Organometallics* **2009**, *28*, 1838–1844. (i) Milanov, A. P.; Thiede, T. B.; Devi, A.; Fischer, R. A. *J. Am. Chem. Soc.* **2009**, *131*, 17062–17063. (j) Milanov, A. P.; Toader, T.; Parala, H.; Barreca, D.; Davide, G. A.; Bock, C.; Becker, H.-W.; Ngwashi, D. K.; Cross, R.; Paul, S.; Kunze, U.; Fischer, R. A.; Devi, A. *Chem. Mater.* **2009**, *21*, 5443–5455. (k) Chen, T.; Hunks, W.; Chen, P. S.; Xu, C.; Di Pasquale, A. G.; Rheingold, A. L. *Organometallics* **2010**, *29*, 501–504. (l) Milanov, A. P.; Xu, K.; Laha, A.; Bugiel, E.; Ranjith, R.; Schwendt, D.; Osten, H. J.; Parala, H.; Fischer, R. A.; Devi, A. *J. Am. Chem. Soc.* **2010**, *132*, 36–37.

(25) (a) Wild, U.; Roquette, P.; Kaifer, E.; Mautz, J.; Wadepohl, H.; Himmel, H.-J. *Eur. J. Inorg. Chem.* **2008**, 1248–1257. (b) Peters, A.; Wild, U.; Hübner, O.; Kaifer, E.; Mautz, J.; Himmel, H.-J. *Chem.—Eur. J.* **2008**, *14*, 7813–7821. (c) Wild, U.; Hübner, O.; Maronna, A.; Enders, M.; Kaifer, E.; Wadepohl, H.; Himmel, H.-J. *Eur. J. Inorg. Chem.* **2008**, 4440–4447. (d) Peters, A.; Kaifer, E.; Himmel, H.-J. *Eur. J. Org. Chem.* **2008**, 5907–5914. (e) Domide, D.; Neuhäuser, C.; Kaifer, E.; Wadepohl, H.; Himmel, H.-J. *Eur. J. Inorg. Chem.* **2009**, 2170–2178. (f) Peters, A.; Trumm, C.; Reinmuth, M.; Emeljanenko, D.; Kaifer, E.; Himmel, H.-J. *Eur. J. Inorg. Chem.* **2009**, 3791–3800. (g) Vitske, V.; König, C.; Kaifer, E.; Hübner, O.; Himmel, H.-J. *Eur. J. Inorg. Chem.* **2010**, 115–126. (h) Emeljanenko, D.; Peters, A.; Wagner, N.; Beck, J.; Kaifer, E.; Himmel, H.-J. *Eur. J. Inorg. Chem.* **2010**, 1839–1846. (i) Trumm, C.; Hübner, O.; Kaifer, E.; Himmel, H.-J. *Eur. J. Inorg. Chem.* **2010**, 3102–3108.

(26) Kawahata, M.; Yamaguchi, K.; Ito, T.; Ishikawa, T. *Acta Crystallogr., Sect. E: Struct. Rep. Online* **2006**, *E62*, o3301–o3302.

(27) Raab, V.; Kipke, J.; Gschwind, R. M.; Sundermeyer, J. *Chem.—Eur. J.* **2002**, *8*, 1682–1693.

(28) Pruszynski, P.; Leffek, K. T.; Borecka, B.; Cameron, T. S. *Acta Crystallogr., Sect. C: Cryst. Struct. Commun.* **1992**, *C48*, 1638–1641.

(29) Roquette, P.; Maronna, A.; Peters, A.; Kaifer, E.; Himmel, H.-J.; Hauf, C.; Herz, V.; Scheidt, E.-W.; Scherer, W. *Chem.—Eur. J.* **2010**, *16*, 1336–1350.

Scheme 1. Bisguanidine Complexes Studied in This Work

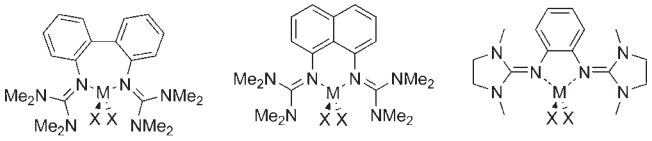

[(btmgbp)MX$_2$] [(btmgn)MX$_2$] [(bdmegb)MX$_2$]

1a M = Ni, X = Cl **2a** M = Ni, X = Cl **3a** M = Ni, X = Cl
1b M = Ni, X = Br **2b** M = Ni, X = Br **3b** M = Ni, X = Br
1c M = Zn, X= Cl **2c** M = Zn, X= Cl **3c** M = Zn, X= Cl

(*N*,*N*′-bis-tetramethylguanidino-benzene),[26] btmgn (*N*,*N*′-bis-tetramethylguanidino-naphthalene)[27] and btmgbp (*N*,*N*′-bis-tetramethylguanidino-biphenyl)[28] as chelating ligands.[29] Therein, we describe the structural, electronic, and magnetic properties of the chloro- and bromo-complexes [(btmgbp)NiX$_2$] (**1**) and [(btmgn)NiX$_2$] (**2**) (see Scheme 1), as well as those of [(btmgb)NiX$_2$] (X = Cl or Br). In addition, we analyzed the fluxional processes of a series of related diamagnetic Zn, Mg, and Al complexes of the btmgn and btmgb ligands, using variable-temperature NMR spectroscopy, combined with line shape analysis, to determine the rate constants and activation enthalpies of the dynamic processes.[30]

Here, we report on a comprehensive ^{1}H and ^{13}C NMR analysis of the paramagnetic nickel(II) complexes **1** and **2**, as well as **3** (see Scheme 1), where the latter features the bridged guanidine bdmegb (*N*,*N*′-bis-dimethylethyleneguanidino)-benzene).[31] The complexes were chosen to analyze the effect of variations of the N−Ni−N bond angle and halide on the paramagnetic NMR shifts. To understand the fluxional processes of these complexes, we combined paramagnetic NMR spectra (including high-resolution ^{13}C−^{1}H correlation experiments) with density functional theory (DFT) calculations to assign all signals unambiguously. This analysis is the prerequisite for the subsequent investigation of the dynamic behavior of the compounds. Most importantly, the kinetics of fast fluxional processes within the paramagnetic complexes—namely, the flipping of the metal from one side of the ligand aromatic plane to the other—is studied in detail via dynamic NMR. It is shown that NMR can be used to study fast fluxional processes in paramagnetic compounds at relatively high temperatures (because of the large signal dispersion). This could lead to the situation that a fluxional process involving the ligand can be observed in paramagnetic complexes, but not in related diamagnetic complexes.

2. Theoretical Background

As sketched in Scheme 1, all of the presented complexes exhibit a distorted tetrahedral coordination geometry that leads to an $S = 1$ ground state, in agreement with magnetic measurements (SQUID) and the results of quantum chemical (DFT) calculations.[29] The SQUID experiments also indicate that, in the temperature region of the NMR experiments (−90 to 30 °C), no spin crossover has to be expected (tetrahedral versus square planar), at least in the solid state.

The assignments of the NMR signals lean on the physicomathematical background of hyperfine coupling between the unpaired electron and the observed nuclei, as outlined briefly in the following.

The experimental chemical shift follows eq 1,[2f,32,33]

$$\delta_{\mathrm{obs},T} = \delta_{\mathrm{orb}} + \delta_{\mathrm{HF},T} = \delta_{\mathrm{orb}} + \frac{S(S+1)\beta_e}{3kT\gamma_N} gA \quad (1)$$

where S is the spin multiplicity, β_e the Bohr magneton, γ_N the nuclear gyromagnetic ratio, and g the **g**-tensor, and A the hyperfine tensor. The observed chemical shift ($\delta_{\mathrm{obs},T}$) can be expressed as the sum of the temperature-independent orbital term (δ_{orb}) and the temperature-dependent hyperfine term ($\delta_{\mathrm{HF},T}$). The orbital term is analogous to the shift of diamagnetic compounds and can be estimated experimentally with the help of closely related closed-shell molecules (e.g., Zn complexes in this work; see below) or from quantum mechanical calculations. The hyperfine shift ($\delta_{\mathrm{HF},T}$) depends on **g** and **A**, which also are relevant for electron paramagnetic resonance (EPR) spectroscopy. Both **g** and **A** can be written as 3 × 3 matrices with isotropic and anisotropic tensors. The product of the two matrices gives a variety of terms, some of which are purely isotropic, purely anisotropic, or both isotropic and anisotropic. Although this leads to many contributions to the hyperfine term ($\delta_{\mathrm{HF},T}$), some of which are difficult to determine purely on the basis of experiments, many experimental data have shown that two terms—namely, the Fermi-contact term (δ_{con}) and the dipolar interaction—dominate the paramagnetic shift, even for $S > {}^1/_2$ systems.[2,5,32,33] DFT calculations, applying the recent general theory of the chemical shift in paramagnetic compounds, support these experimental observations.[34] Consequently, the hyperfine term can be approximated by eq 2:

$$\delta_{\mathrm{HF},T} \cong \delta_{\mathrm{con}} + \delta_{\mathrm{dip}} \quad (2)$$

The strong distance dependence of the dipolar contribution leads to dipolar shifts[35] of a few ppm only for atoms further apart from the paramagnetic center, which is usually the metal atom. Consequently, the Fermi-contact term may dominate the chemical shift if organic ligands are covalently bound to metals with unpaired d-electrons.

The Fermi-contact term (δ_{con}) is transmitted through covalent chemical bonds and induces residual spin density $\rho_{\alpha\beta}$, which is directly proportional to δ_{con}:[2,4,32,33]

$$\delta_{\mathrm{con}} = \frac{\mu_0 {\mu_B}^2 {g_E}^2 (S+1)}{9kT} \rho_{\alpha\beta} \quad (3)$$

Herein, μ_0 denotes the permeability of a vacuum ($4\pi \times 10^{-7}$ N/A), μ_B the Bohr magneton (9.274015×10^{-24} J/T), g_E the free-electron g-factor ($g_E = 2.0023$), S the total spin, k the Boltzmann constant (1.380658×10^{-23} J/K), and T the absolute temperature (in Kelvin). Therefore, the relationship between

(30) Reinmuth, M.; Wild, U.; Rudolf, D.; Kaifer, E.; Enders, M.; Wadepohl, H.; Himmel, H.-J. *Eur. J. Inorg. Chem.* **2009**, 4795–4808.
(31) Roquette, P.; König, C.; Hübner, O.; Wagner, A.; Kaifer, E.; Enders, M.; Himmel, H.-J. *Eur. J. Inorg. Chem.* **2010**, 4770–4782.
(32) Bertini, I.; Luchinat, C.; Parigi, G. *Solution NMR of Paramagnetic Molecules—Applications to Metallobiomolecules and Models*; Elsevier: Amsterdam, 2001.
(33) Jesson, J. P. The Paramagnetic Shift. In *NMR of Paramagnetic Molecules—Principles and Applications*; La Mar, G. N., Horrocks, W. DeW., Jr., Holm, R. H., Eds.; Academic Press: New York, London, 1973.
(34) (a) Pennanen, T. O.; Vaara, J. *Phys. Rev. Lett.* **2008**, *100*, 133002. (b) Liimatainen, H.; Pennanen, T. O.; Vaara, J. *Can. J. Chem.* **2009**, *87*, 954–964.
(35) The molecular tumbling in solution leads to an averaged dipolar shift contribution, which is often named pseudocontact shift.

the Fermi-contact shift and the spin density can be expressed as a collection of physical constants:

$$\delta_{\mathrm{con}} = m\frac{(S+1)}{T}\rho_{\alpha\beta} \tag{4}$$

with

$$m = \frac{\mu_0\mu_B{}^2 g_E{}^2}{9k} = 23.5\times10^6 \text{ ppm K a.u.}^{-1} \tag{5}$$

In the constant m, the conversion factor from the SI unit to atomic units ($a_0 = 52.9177\times10^{-12}$ m) and to ppm was taken into account.[4,7] This formula is strictly only valid for systems without zero-field splitting, which may not deviate from Curie-type ($1/T$) behavior.[4,36] However, Kurland and McGarvey have noted that the Fermi-contact shift (described by eq 4), even in the presence of zero-field splitting, may still be a good approximation.[36] This is important because all complexes studied in this work show a significant zero-field splitting of 20−30 cm^{-1}.[29]

The proportionality between the Fermi-contact shift and the spin density leads to a distinct shift pattern in the NMR spectra, which depends on the nature of the atomic orbitals interacting with their neighbors. The spin density may be delocalized through the skeleton of the ligand either by σ- or π-bonds. In many cases, the signals of the observed nuclei alternate in the way high-field−low-field−high-field or vice versa, resulting from an alternating spin density at each nucleus. Particularly in heteroaromatic ligands, this effect is very distinctive. Therein, the spin density in the p_z orbital of a carbon atom affects the distribution of the two paired electrons in the sp^2-orbital at this carbon (e.g., of the C−H bond) in such a way, that the spin density on the adjacent proton is of opposite sign. Moreover, the spin density at the next adjacent aromatic carbon is also of opposite sign. As a result, the spin densities of two neighboring hydrogen atoms have opposite signs.

The observability of NMR transitions in paramagnetic molecules depends on the relaxation behavior of the measured NMR nucleus, which itself is strongly dependent on the electron relaxation rate and the magnetic interaction between the electron and nuclear spin. As a rule of thumb, well-resolved NMR lines can be obtained when the electron spin−lattice relaxation rate ($T_{1e}{}^{-1}$) is fast, compared to the electron−nucleus hyperfine interaction A.[37] Very narrow NMR lines are possible when $T_{1e}{}^{-1} \approx (A/\hbar)^2$, which is the case for several high-spin Co(II) and Ni(II) complexes ($T_{1e} \approx 10^{-12}$ s).[38] Typically, the NMR linewidths within one NMR spectrum increase as the paramagnetic shift contribution increases. However, additional line broadening of some signals may occur, because of efficient dipolar electron−nucleus relaxation. In the fast motion limit, the nucleus relaxation rates $T_{1N}{}^{-1}$ and $T_{2N}{}^{-1}$ are equal and can be determined from the signal line width ($T_{2N}{}^{-1} = \pi\Delta\nu_{1/2}$). From eq 6, it is obvious that the dipolar relaxation rate depends on r^{-6} (r is the through-space distance between the unpaired electron and the observed nucleus).[39] This strong distance dependence allows the assignment of additionally broadened NMR signals to nuclei close to the metal center.

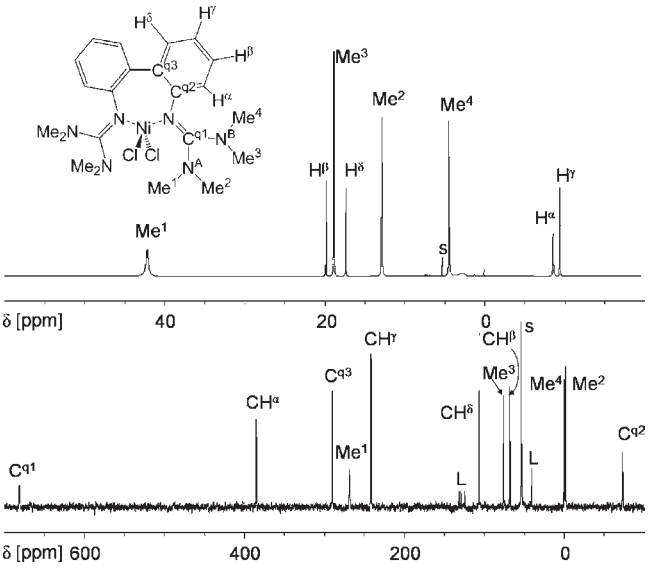

Figure 1. ^{1}H NMR spectrum at 600 MHz (top) and ^{13}C{^{1}H} NMR spectrum at 150 MHz (bottom) for **1a** (22 °C, CD_2Cl_2; "S" and "L" respectively denote signals from the solvent and traces of uncoordinated ligand).

$$\frac{1}{T_{1(N)}} = \frac{1}{T_{2(N)}} = \frac{4S(S+1)\gamma_N{}^2 g^2\beta^2 T_{1e}}{r^6} \tag{6}$$

3. NMR Experiments and Signal Assignment

All the paramagnetic Ni(II) complexes in this study give well-resolved NMR spectra. This is due to a fast electron relaxation and, consequently, a relatively slow NMR relaxation, as outlined above. All expected ^{1}H NMR signals are observed with relatively narrow line widths (e.g., 20−180 Hz for **1a** at 22 °C) The advantageous relaxation behavior of the Ni complexes also allows the direct detection of ^{13}C NMR spectra. Optimized repetition times in combination with a cryogenically cooled ^{13}C detection probe leads to good ^{13}C NMR spectra within 5−60 min (see the Experimental and Computational Details section for details). The following discussion and signal assignment is based on the analysis of chemical shifts, intensities, relaxation behavior, and C,H correlation data, as well as DFT calculated spin density distributions.

1a and 1b. Figure 1 displays the ^{1}H and ^{13}C NMR spectra recorded for **1a** (see Supporting Information for VT-NMR experiments). At 22 °C, the ^{1}H NMR spectrum consists of a broad signal at 42.2 ppm for Me^1 and two groups of resonances, of which the larger exhibits maxima at 18.9, 12.9, and 4.5 ppm, attributable to Me^3, Me^2, and Me^4, respectively. The aromatic backbone of the ligand is responsible for the second, less-intense group of signals. Herein, the signals at 19.9 and 17.4 ppm, as well as those at −8.5 and −9.4 ppm, can be assigned to H^β, H^δ, H^α, and H^γ, respectively. The integral ratio of 3:1:3:1:3:3:1:1 is in good agreement with the overall number of 32 protons in the C_2 symmetry molecule. As outlined previously, the

(36) Kurland, R. J.; McGarvey, B. R. *J. Magn. Reson.* **1970**, *2*, 286–301.
(37) (a) The condition $T_{1e}{}^{-1} \gg A/\hbar$ is necessary to collapse the multiplet structure of the NMR transition. This criterion is necessary but does not guarantee narrow NMR lines. For a comprehensive discussion, see: (b) refs 2a or 33.
(38) Bertini, I.; Luchinat, C. In *NMR of Paramagnetic Molecules in Biological Systems*; Benjamin/Cummings: Menlo Park, CA, 1986.
(39) Swift, T. J. The Paramagnetic Linewidth. In *NMR of Paramagnetic Molecules—Principles and Applications*; La Mar, G. N., Horrocks, W. DeW., Jr., Holm, R. H., Eds.; Academic Press: New York, London, 1973.

Table 1. Chemical Shift (δ) and Longitudinal (Spin−Lattice) Relaxation Time (T_1) for ^{1}H at −40 °C (200 MHz, CD_2Cl_2)

	1a		1b		2a		2b		3a		3b	
	δ [ppm]	T_1 [ms]	δ [ppm]	T_1 [ms]	δ [ppm]	T_1 [ms]	δ [ppm]	T_1 [ms]	δ [ppm]	T_1 [ms]	δ [ppm]	T_1 [ms]
H^{α}	−13.2	27.3	−16.0	4.9	−7.9	29.9	−11.0	11.1	9.2	63.2	9.8	62.7
H^{β}	23.7	137.3	23.4	69.4	29.7	231.5	29.8	125.0	5.4	*a*	4.7	354.5
H^{γ}	−13.9	268.4	−14.2	83.4	−12.7	170.5	−10.7	74.0				
H^{δ}	21.0	78.5	20.3	66.9								
Me^1	55.7	3.5	36.8	2.8	64.4	4.0	43.3	2.2				
Me^2	16.0	29.4	17.4	18.0	32.0	28.3	34.0	17.2				
Me^3	23.1	98.6	23.0	52.9	38.9	69.2	37.8	40.4				
Me^4	3.7	50.1	6.4	27.5	19.0	23.6	21.2	9.6				
Me									57.9	8.9	52.1	12.6
$-CH_2-$									59.3	43.7	63.7	81.5
$-CH_2-$									59.6	52.5	67.1	88.0

[a] At −40 °C, the measurement of T_1 is hampered due to overlapping of the resonance with the signal due to the CD_2Cl_2 solvent.

Fermi-contact interaction governs the observed chemical shifts in the case of the aromatic protons. The spin density residing in the aromatic ring system (see Figure 9, presented later in this work) leads to a deshielding of the proton next to the paramagnetic center (H^{α}) and, thus, to a low-field shift of this resonance. In addition, this signal becomes relatively broad (compared to H^{β} and H^{δ}), in accordance with a shorter distance to the unpaired electrons at the Ni(II) and, hence, a faster dipolar relaxation of the ^{1}H nuclei. Because of the r^{-6} dependence of the dipolar relaxation, this effect is much weaker for the other ^{1}H resonances. An even number of bonds connect the metal with the atoms of H^{α}. Therefore, the second high-field shifted peak must be assigned to H^{γ} (also for an even number of bonds). The chemical shifts, as well as the line widths, of the signals due to H^{β} and H^{δ} are similar.

For diamagnetic systems, the observation of homonuclear *J*-coupling in the H,H-COSY spectra is often used for verification of the assignment. However, the observation of cross peaks in 2D spectra of paramagnetic compounds is generally hampered by fast relaxation processes. The spin system may relax completely during the evolution time. The evolution time needed for the observation of cross peaks is proportional to J^{-1}. Thus, only large couplings are observable when short evolution times are used. In the case of **1a**, the relatively slow relaxation of the aromatic protons, combined with a ^3J-coupling constant of ∼6 Hz, allows for the detection of cross peaks in H,H-COSY experiments (see the Supporting Information). Therefore, in this way, the ^{1}H resonances that are due to H^{β} and H^{δ} of **1a** can be assigned unambiguously.

For a definite assignment of the Me protons, the orientation of the guanidino moieties must be taken into account. Because of restricted rotations around the C−N bonds, all methyl groups within a guanidino unit are inequivalent, resulting in a total of four resonances in the ^{1}H NMR spectra. Hereby, the dipolar interaction between the ^{1}H nuclei and the metal-centered electron spins (r^{-6} dependence of nuclear relaxation; see above) causes faster relaxation of the H atoms, which are close to the Ni(II) center. Consequently, the signal at 42.2 ppm should belong to the methyl group Me^1. The assignment of the remaining three signals is achieved with the aid of quantum chemical (DFT) calculations, as discussed below. The resonance with the smallest hyperfine shift (located in the "diamagnetic region", i.e. δ = 0−10 ppm) can then be assigned to Me^4 (δ = 4.5 ppm). The signals at 18.9 and 12.9 ppm are assigned to Me^3 and Me^2, respectively. The assignment is supported by the observed T_1 relaxation times, which are listed in Table 1.

Subsequently ^{13}C NMR measurements at various temperatures were conducted for **1a**. As anticipated, the temperature dependency of the signals turns out to be similar to that in the ^{1}H NMR spectra (see Figure 1 for data obtained at 22 °C and Figure S5 in the Supporting Information for the VT-NMR data). The assignment of the peaks relies on a series of ^{13}C NMR experiments with selective ^{1}H decoupling (see Figure 2) and the temperature dependence of all signals in the VT-NMR spectra (see the Curie plots in Figure 3).

The aromatic carbon atoms, which are bound to the high-field shifted protons H^{α} and H^{γ}, are the authors of the resonances at 384.9 (CH^{α}) and 241.4 ppm (CH^{γ}). The other two aromatic carbons CH^{δ} and CH^{β} give rise to signals at 105.9 and 68.1 ppm, respectively. The two quartets due to the carbon atoms of the methyl groups Me^2 and Me^4 partially overlap. Selective decoupling allows the assignment of the peak at −0.3 ppm to Me^4 and that at −1.7 ppm to Me^2. The signals of the other two methyl groups occur at 268.5 (Me^1) and 75.7 ppm (Me^3). The three quaternary carbon atoms show at 681.0, 290.0, and −72.7 ppm. As already mentioned, the spin density in aromatic π-systems changes its sign for adjacent carbon atoms and also for a carbon atom and the hydrogen atoms bonded to it. This typical behavior is clearly visible in the spectrum (see Figure 9 in the Comparison between Experimentally Determined and Calculated Paramagnetic Shifts section of this paper). Because of a negative shift of H^{α} (corresponding to negative spin density), the spin density at C^{q2} should also be negative. Consequently, the corresponding resonance should exhibit a high-field paramagnetic shift and the signal at −72.7 ppm must be assigned to C^{q2} ($\delta^{exp}_{HF,T} = \delta^{exp}_{obs} - \delta_{orb} = -221.1$ ppm; δ^{exp}_{obs} is the observed experimental shift and is identical to δ described in the Experimental and Computational Details section or given in the tables). The adjacent atom C^{q3} is one bond further away from the Ni(II) center and therefore should exhibit a positive spin density, which is however smaller than that on C^{q2}. Therefore, the signal at 290.0 ppm belongs to C^{q3} ($\delta^{exp}_{HF,T}$ = 153.1 ppm). The quaternary guanidino carbon atom (C^{q1}) gives rise to the ^{13}C NMR signal with the largest paramagnetic shift at δ = 681.0 ppm.

The assignment of the ^{13}C resonances is supported by analysis of their temperature dependence. For all chemical

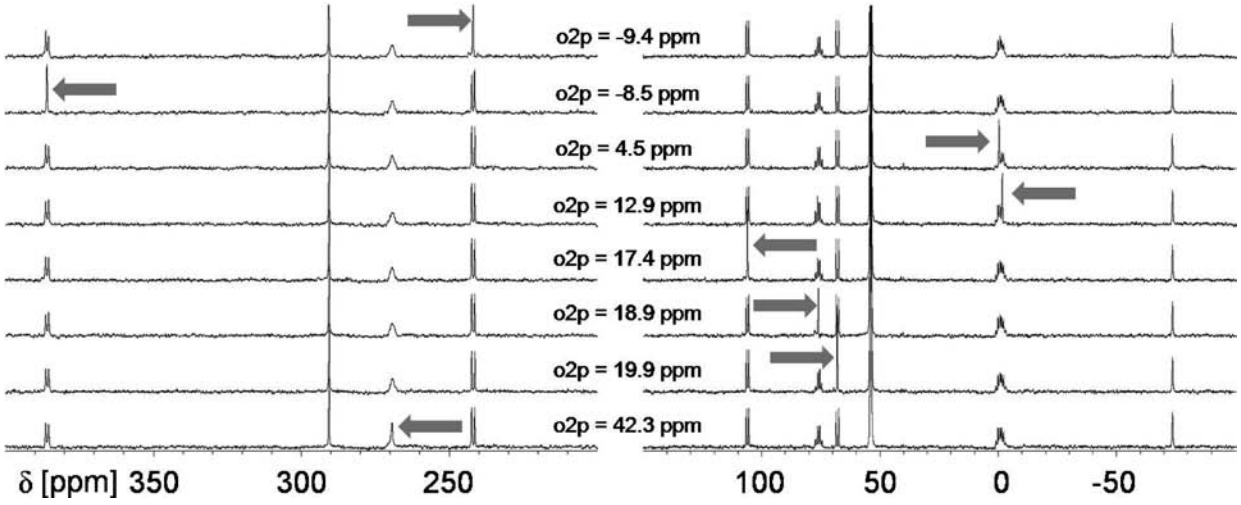

Figure 2. ^{13}C NMR spectra of **1a** (22 °C, 150 MHz, CD_2Cl_2) with selective ^1H decoupling (o2p = frequency offset of ^1H-decoupler). The arrows highlight the decoupled ^{13}C signals.

shifts δ, a linear T^{-1} relationship was found, in accordance with Curie-type behavior (see Figure 3). An increase in the temperature leads to a displacement of all resonances in the direction toward the diamagnetic region. Depending on the spin density at the observed nucleus, this movement is either positive or negative on the δ scale. The signal with the largest low-field shift shows the strongest temperature dependence in the Curie plot (C^{q1} at 681.0 ppm). While the aromatic protons of CH^{β} and CH^{δ} move toward the region typical for aromatic diamagnetic carbons, the resonance of Me^3 shifts to smaller ppm values, leading to an almost-complete overlap of the signals attributable to CH^{β} and Me^3 at higher temperatures.

The ^1H NMR spectra recorded for the chloro- and the bromo-complexes **1a** and **1b** show two considerable differences (see Table 2 and Supporting Information for VT-NMR). The Me^1 protons in **1b** are much less-shifted than in **1a** (28.6 ppm compared to 42.2 ppm). In addition, the resonance due to the aromatic proton H^{α} is more shifted (−10.6 ppm). All ^1H resonances can be assigned in a similar way to those of **1a**. The protons of Me^2, Me^3, and Me^4 are the authors of the resonances at 14.0, 18.8, and 6.4 ppm, respectively. The peaks for the aromatic protons occur at 19.6, −9.6, and 14.0 ppm for H^{β}, H^{γ}, and H^{δ}, respectively. The H,H-COSY experiments (see the Supporting Information) fully support the assignment of the aromatic protons.

The longitudinal relaxation time (T_1) measurements for all signals of **1a** and **1b** are also consistent with the assignment (Table 1). Hereby, the resonances that are due to the Me^1 groups of both complexes relax 1 order of magnitude faster than those of the other methyl groups. Moreover, the relaxation time of the aromatic protons increases in the order $H^{\alpha} < H^{\beta} < H^{\gamma}$. These results are in accordance with the strong distance dependence of dipolar relaxation (see eq 6). The relaxation time T_1 correlates quite well with r^6, where r is the distance between the Ni atom and the corresponding H atoms (see the correlation plot in the Supporting Information).

2a and 2b. The change of the ligand system from btmgbp to btmgn brings about a smaller N−Ni−N bite angle and a planar aromatic backbone. Thus, not surprisingly, the fluxional behavior of the guanidino Me groups also varies. While **1a** and **1b** are rigid on the NMR time scale at room temperature (i.e., four distinct Me resonances), **2a** (X = Cl) and **2b** (X = Br) are fluxional. Only the aromatic protons at 24.0, −4.4, and −8.2 ppm are well-resolved in the NMR spectra of **2a** recorded at 30 °C (see Figure 4). The methyl protons now give rise to three broad signals, at 47.7, 28.1, and 15.0 ppm. However, at 20 °C, splitting of the broad central signal into two separate peaks is already visible, and at −80 °C, all methyl proton signals sharpen to discrete peaks at 80.2, 47.2, 38.3, and 23.0 ppm. Moreover, all methyl protons and the aromatic proton signal due to H^{β} are shifted to low field (34.8 ppm), whereas the aromatic signals due to H^{α} (10.3 ppm) and H^{γ} (16.5 ppm) sense a high-field shift. The assignment of the signals can be accomplished in a similar way as that for **1a** and **1b**, again under the assumption of the leading role of the Fermi-contact interaction. Integration of the signals at −80 °C returns the expected 3:3:3:1:3:1:1 ratio. The variable-temperature NMR measurements show that the signals at 47.2 (Me^3) and 38.3 ppm (Me^2), as well as the signals at 80.2 (Me^1) and 23.0 ppm (Me^4), are exchanging. This exchange interconverts the groups Me^1 with Me^4 and Me^2 with Me^3, respectively (see discussion below).

For all signals, the chemical shift δ is plotted as a function of T^{-1} over the temperature range from −90 °C to 30 °C (see Figure 5). For temperatures up to 10 °C, all signals exhibit typical Curie-type behavior. However, above 10 °C, dynamic effects are responsible for deviations from this behavior. Especially, the exchange interaction between Me^2 and Me^3, which will be discussed below, can clearly be observed here.

The dynamic behavior, as visible in the ^1H NMR spectra of **2a** at room temperature, is not observable in the ^{13}C NMR spectra. This can be explained by the larger signal dispersion in the paramagnetic ^{13}C NMR spectra, leading to higher coalescence temperatures. All signals can be assigned following the same procedures as those for **1a**. Thus, at a temperature of 22 °C, C^{q1} appears at 681.5 ppm and the signal due to C^{q2} is strongly high-field-shifted to −179.7 ppm. The signal of the C^{q3} carbon is located at 262.1 ppm and that of C^{q4} at 0.4 ppm. The signals of the

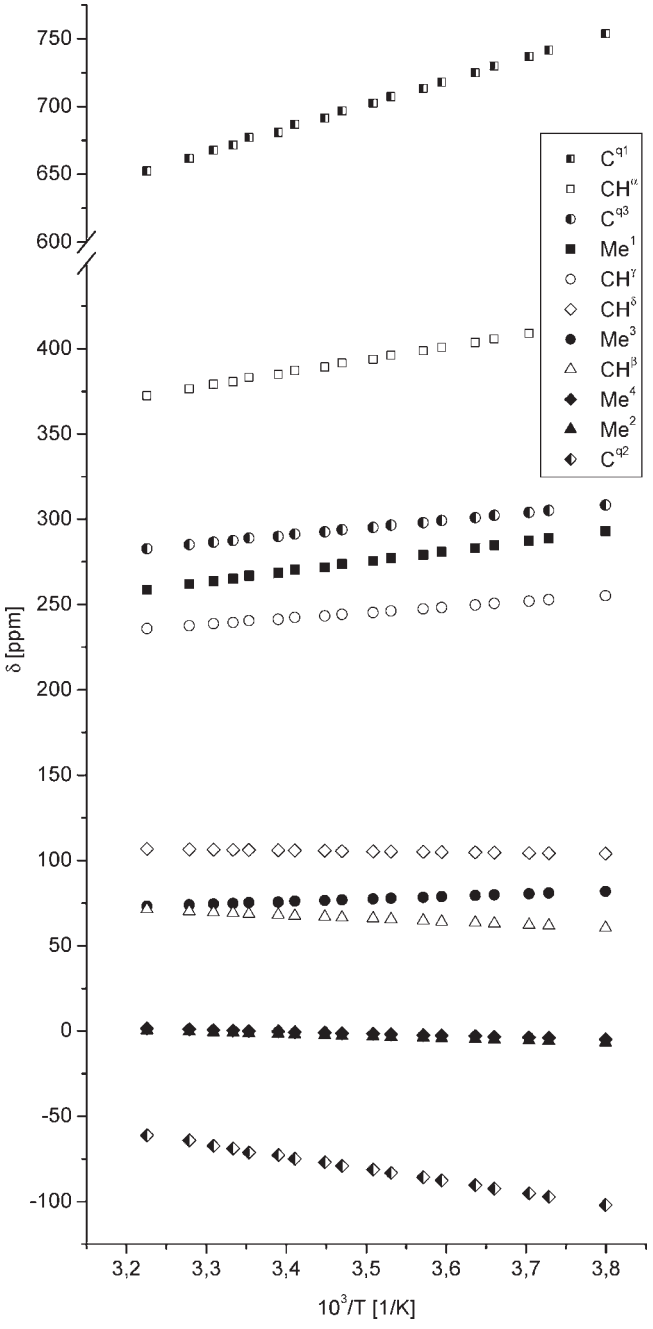

Figure 3. Curie-plot of the ^{13}C NMR data for **1a**. Solid, open and half-filled data points represent the signal positions of the methyl carbons, aromatic carbons, and quaternary carbon atoms, respectively.

Table 2. ^{1}H NMR Chemical Shifts δ for **1a** and **1b** at 22 °C (600 MHz, CD_2Cl_2)

	δ [ppm]							
compound	H^{α}	H^{β}	H^{γ}	H^{δ}	Me^1	Me^2	Me^3	Me^4
1a	−8.5	19.9	−9.4	17.4	42.2	12.9	18.9	4.5
1b	−10.6	19.6	−9.6	14.0	28.6	14.0	18.8	6.4

aromatic CH groups (CH^{α}, CH^{β}, and CH^{γ}) are found at 683.7, 114.1, and 218.1 ppm, respectively. The signals of the methyl protons are assigned as Me^1 for the most low-field-shifted peak at 224.6 ppm, Me^3 at 20.3 ppm, Me^2 at −17.1 ppm, and Me^4 at −5.3 ppm (see the Supporting Information for spectra).

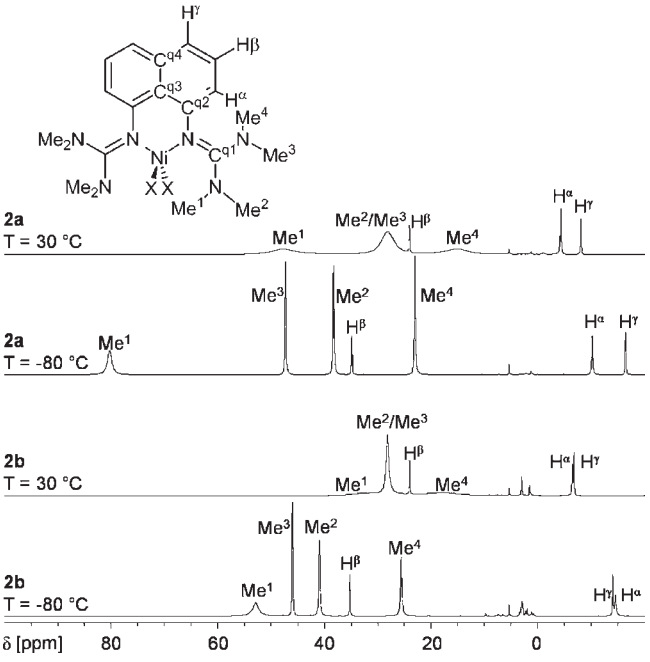

Figure 4. ^{1}H NMR spectra of **2a** and **2b** (200 MHz, CD_2Cl_2).

In the ^{1}H NMR spectra, the bromo derivative **2b** shows a temperature dependence that is analogous to that of the chloro derivative **2a** (see Figure 4 and the Supporting Information). At 30 °C, only the aromatic protons give rise to well-resolved signals at 24.0, −6.6, and −6.8 ppm for H^{β}, H^{α}, and H^{γ}, respectively. The methyl protons Me^1 and Me^4 are visible as two extremely broad signals (31.7 ppm and 17.5 ppm), and the methyl groups Me^2 and Me^3 give one signal at 28.1 ppm. By decreasing the temperature to 10 °C, this signal splits into two resonances. With further decreases in temperature, the signals become sharper, but below −30 °C, all peaks are broadened again, by virtue of their paramagnetism. From the linewidth of the aromatic signals and the Curie plot (see the Supporting Information), it is obvious that the resonance due to H^{α} is more temperature-sensitive than that due to H^{γ}. This leads to the observed crossing of both signals (in the temperature range from 10 °C to −20 °C). At −80 °C, the signals of **2b** show a similar pattern than those of **2a** (see Figure 4). Integration over all signals returns a 3:3:3:1:3:1:1 ratio, as anticipated for the btmgn ligand of **2a**.

A comparison of the longitudinal relaxation times T_1 for **2a** and **2b** finds all T_1 values of **2b** to be shorter, by a factor of 2−3, compared with **2a**, but with a similar overall trend for both molecules (see Table 1). Both in **2a** and **2b**, the shortest relaxation time was measured for the protons of Me^1, followed by their exchange partners from Me^4. The signals due to Me^2 and Me^3 both have larger T_1 values. The aromatic proton closest to the paramagnetic center, H^{α}, exhibits a T_1 value of the same order than that of Me^4. For both complexes, the resonances due to H^{β}, which has the largest distance to the paramagnetic nickel center, have the longest relaxation times.

3a and 3b. Exchanging the btmgn ligand with the bdemgb ligand, a similar symmetry results; however, the bite angle of the ligand becomes smaller. In addition, the rotation around the $C^{q1}-N_{amine}$ bonds is now blocked. Figure 6 shows the ^{1}H and ^{13}C NMR spectra recorded for

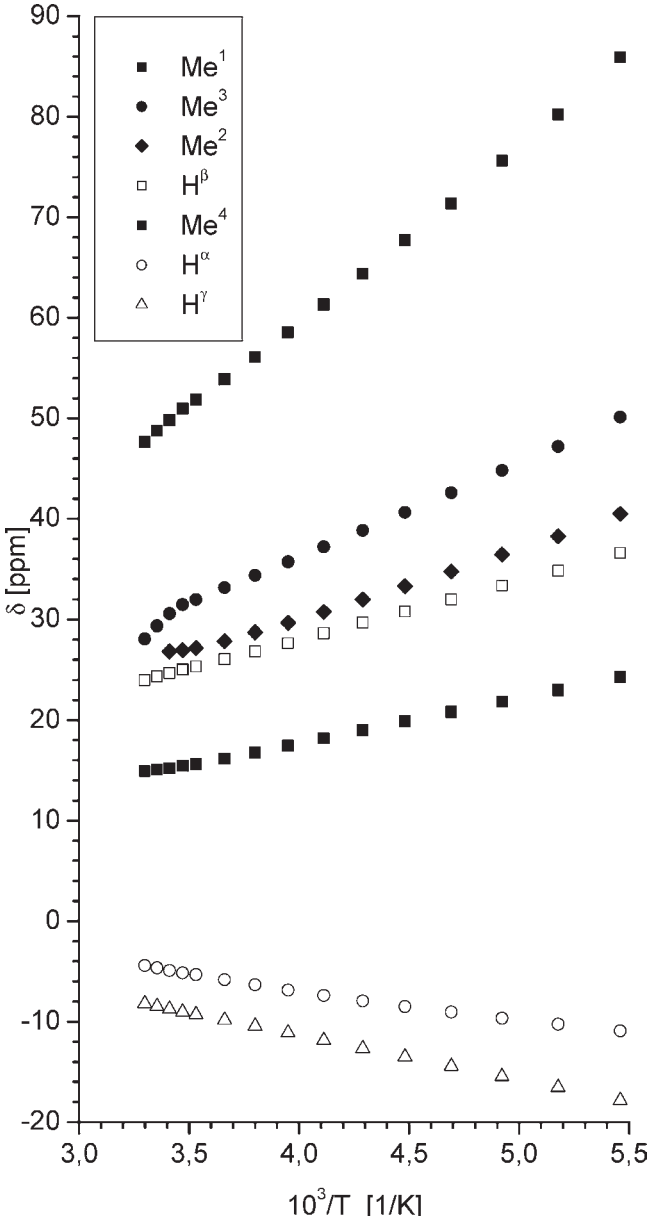

Figure 5. Curie plot of the ^{1}H NMR data for **2a**. Solid and open data points represent the methyl and aromatic protons, respectively.

[(bdmegb)NiCl$_2$], **3a** (see the Supporting Information for the ^{1}H VT-NMR data). At room temperature, the fast exchange of the two N−Me groups leads to the detection of just one signal for the methyl groups in the ^{1}H and ^{13}C NMR spectra. The same holds for the CH_2 groups, which give one signal in the ^{13}C NMR and two signals in the ^{1}H NMR spectrum. The signals of the aromatic protons experience only a slight paramagnetic shift and appear in the diamagnetic region at 9.9 ppm for H^{α} and 4.9 ppm for H^{β}. The obvious explanation is that only a negligible portion of the spin density resides in the aromatic backbone, whereas the electronic environment of H^{α} will be slightly more affected than that of H^{β} (also see the discussion below and Figure 9, given later in this work). In the coupled ^{13}C NMR spectrum, all expected resonances are clearly visible (see Figure 6). The signals for two quaternary carbons appear at 612.3 and −344.5 ppm. In analogy to **1** and **2**, and with the help of DFT calculations (see Table 3

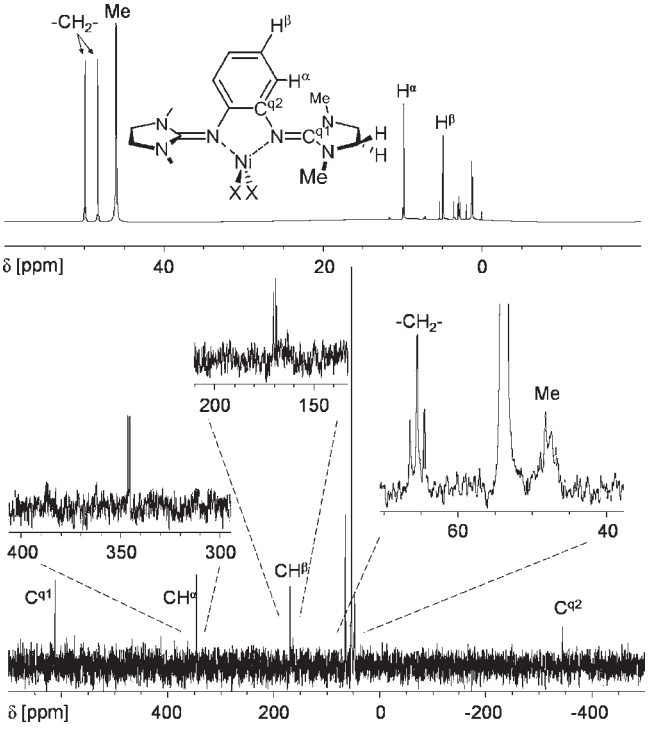

Figure 6. ^{1}H NMR spectrum at 600 MHz (top) and ^{13}C NMR spectrum at 150 MHz (bottom) for **3a** (22 °C, CD_2Cl_2).

and Figure 9 below), the assignment is accomplished such that the peak at low field corresponds to C^{q1}, and that at high field corresponds to C^{q2}. In addition, two doublets at 345.5 and 169.6 ppm are visible, which are assigned to the aromatic carbons CH^{α} and CH^{β}, respectively. Here again, the CH^{β} resonance experiences only a small hyperfine shift. The signal at 65.5 ppm can be allocated on the basis of its triplet pattern to the bridging ethylene carbons. The broad singlet signal at 47.5 ppm belongs to the methyl groups. A 2D ^1J-CH correlation experiment is performed for direct assignment of the proton resonances to the specific carbon signals (see Figure 7). Given the absence of any interaction with the hydrogen atoms, the quaternary carbons can be assigned directly. The aromatic protons interact with the two doublets in the ^{13}C NMR spectrum and can thereby be assigned as outlined above. The methyl protons show a cross peak to the broad singlet, which, again, is consistent with the previous assignment. The triplet in the ^{13}C NMR spectrum clearly interacts with both ^{1}H resonances of the ethylene groups. Therefore, these signals must stem from the two hydrogens bonded to the same carbon atom.

The structurally equivalent complex [(bdmegb)NiBr$_2$], **3b**, exhibits the same characteristics in the ^{1}H NMR spectrum as **3a** (see the Supporting Information), with two signals for the ethylene hydrogens and one resonance for the methyl protons. Again, the signals of the aromatic protons occur close to the diamagnetic region.

The longitudinal relaxation times T_1 for the resonances in **3a** and **3b** are generally similar to those in the complexes **1a**/**1b** and **2a**/**2b**. The methyl group, being closer to the paramagnetic center, relaxes nearly 1 order of magnitude faster than the ethylene protons. The T_1 relaxation time for the ethylene protons is in the same order as that of the aromatic proton H^{α}. In **3b**, the

Table 3. Paramagnetic NMR Shift Data (600 MHz for ^{1}H NMR, 150 MHz for ^{13}C NMR, CD_2Cl_2) and Calculated Fermi-Contact Chemical Shifts at 22 °C

	1a		2a		3a	
	$\delta^{exp}_{HF,T}$[a] [ppm]	δ^{calcd}_{con} [ppm]	$\delta^{exp}_{HF,T}$[a] [ppm]	δ^{calcd}_{con} [ppm]	$\delta^{exp}_{HF,T}$[a] [ppm]	δ^{calcd}_{con} [ppm]
			^{1}H NMR			
H^{α}	−15.1	−19.2	−11.1	−27.1	3.1	1.6
H^{β}	12.6	11.2	17.3	17.6	−1.9	3.2
H^{γ}	−16.5	−19.2	−16.1	−22.3		
H^{δ}	10.3	6.4				
Me^1	38.8	35.1	46.8	22.9		
Me^2	10.2	9.6	23.4	16.5		
Me^3	16.1	17.0	27.9	28.7		
Me^4	2.4	8.5	12.2	13.8		
Me					43.2	19.4
$-CH_2-$					45.1[b]	22.3
			^{13}C NMR			
CH^{α}	259.6	225.0	565.66	510.6	223.9	260.1
CH^{β}	−61.1	−65.4	−9.35	−44.7	48.5	71.8
CH^{γ}	117.1	103.7	91.86	113.3		
CH^{δ}	−30.9	−38.3				
Me^1	223.3	153.2	179.49	121.3		
Me^2	−43.9	−38.3	−59.28	−54.3		
Me^3	35.3	31.9	−20.12	−27.1		
Me^4	−39.4	−41.5	−44.41	−46.3		
Me					11.8	13.6
$-CH_2-$					16.5	19.9
C^{q1}	514.8	453.1	516.12	379.7	448.6	501.0
C^{q2}	−221.1	−210.6	−325.75	−300.0	−483.6	−191.5
C^{q3}	153.1	94.1	123.97	148.4		
C^{q4}			−121.29	−164.3		

[a] $\delta^{exp}_{HF,T}$ is obtained by subtracting the diamagnetic chemical shift from the observed chemical shift, with the analogous Zn complexes as diamagnetic references. [b] Average value.

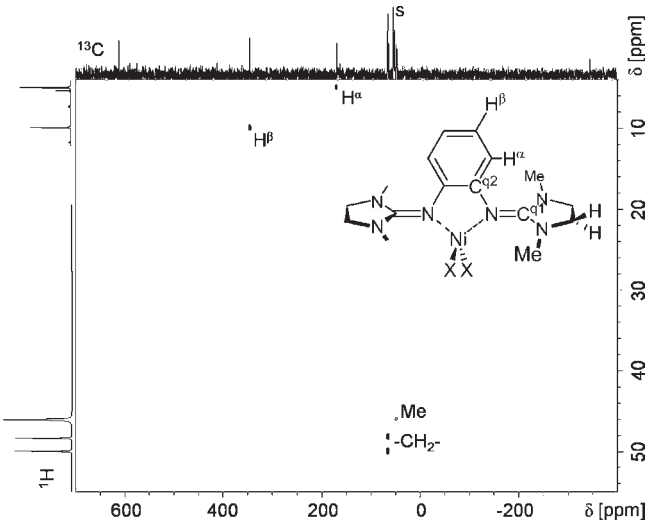

Figure 7. ^1J-CH correlation NMR for **3a** (22 °C, 600 MHz, ^{13}C in direct dimension (F2), CD_2Cl_2, s = solvent).

resonance of H^{β} exhibits the longest relaxation time, which is consistent with its large distance from the paramagnetic center.

4. Comparison between Experimentally Determined and Calculated Paramagnetic Shifts

As outlined above, the chemical shift is the sum of diamagnetic (or orbital) and paramagnetic (or hyperfine) contributions. The hyperfine shift is proportional to the hyperfine coupling constant. If the contact term dominates the hyperfine shift, the spin density can be calculated easily from the observed chemical shift and then compared with quantum chemically calculated spin densities. The experimental hyperfine shifts ($\delta^{exp}_{HF,T}$) of the Ni(II) complexes are obtained by subtracting the diamagnetic chemical shift from the observed chemical shift. The NMR spectra of the analogous Zn(II) complexes (**1c**, **2c**, **3c**) provide us with the diamagnetic chemical shifts. For this purpose, we synthesized these Zn complexes. The details of the synthesis of **1c** and **3c** are given in the Experimental and Computational Details section of this paper, and the synthesis of **2c** was already published previously by us.[30] In Figure 8, the molecular structures, as derived from X-ray diffraction of **1a** vs **1c** and **3a** vs **3c**, are superimposed, showing that the Ni and Zn complexes exhibit similar structural properties.

Quantum chemical (DFT) calculations are carried out for all Ni(II) complexes (**1a**−**3a**). These calculations employ the B3LYP functional, which was recently shown to reliably predict hyperfine shifts,[34b] together with a combination of two different basis sets (see the Experimental and Computational Details section of this paper). The calculated chemical shifts (δ^{calcd}_{con}) caused by the Fermi-contact interaction are obtained by applying eqs 3−5. All chemical shifts are calculated at a temperature of 22 °C. To test our approach, we also carried out an alternative analysis, based on calculated orbital terms for the **2a** complex (see the Supporting Information). However, the comparison between both methods (see the Supporting Information) indicates that the analysis based on the experimental orbital terms derived from the corresponding Zn complexes leads to better results.

Figure 9 shows the DFT calculated envelop maps of the spin densities for the three complexes **1a**, **2a**, and **3a**. Herein,

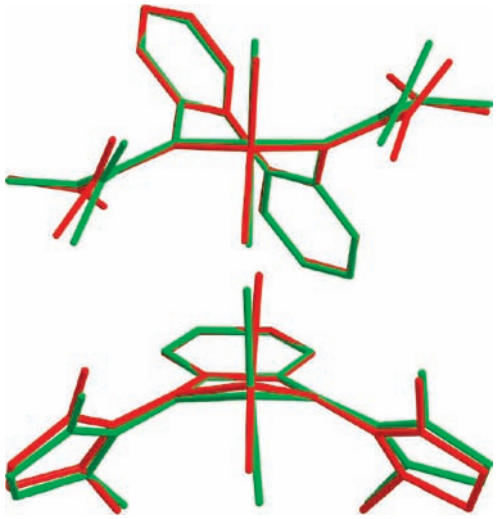

Figure 8. Superimposed molecular structures of the Zn(II) (red) and Ni(II) complexes (green) showing their structural similarity. Top: **1a** and **1c**. Bottom: **3a** and **3c**.

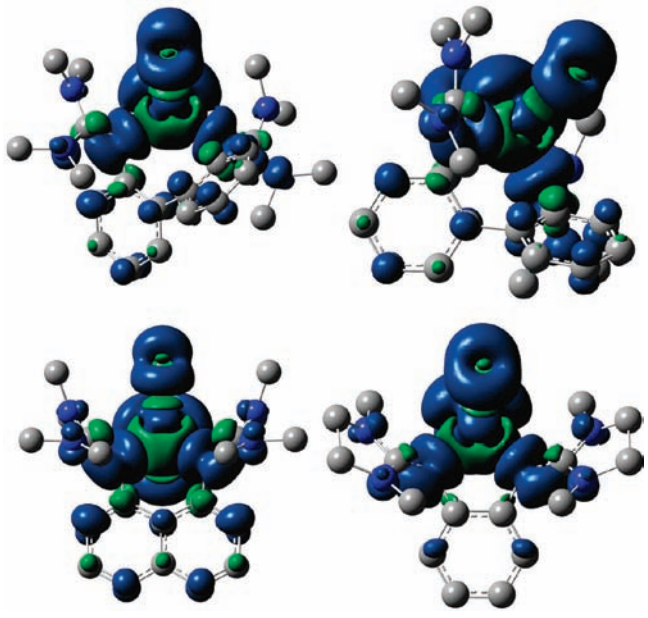

Figure 9. Envelop maps of the spin density $\rho_s(\mathbf{r})$ = 0.0004 a.u. for **1a** (top left: view along the Ni−Cl vector; top right: view on the aromatic plane), **2a** (bottom left), and **3a** (bottom right) (B3LYP/BS-1 level of theory). Hydrogen atoms have been removed for the sake of clarity. (The green and blue colors denote positive and negative spin density, respectively.)

the alternation of the spin density, explicitly in the aromatic system, can be clearly seen. This effect plays an important role for the assignment of the peaks in the NMR spectra, as explained above. The experimentally determined and calculated paramagnetic ^{1}H and ^{13}C NMR shifts are compared in Table 3 (see Figure 10 for an illustration). For all three complexes **1a**−**3a**, the general level of agreement between experiment and calculation is satisfactory, especially for atom centers with relatively high spin density. However, there are also some relatively large discrepancies (see, e.g., H^{α} and Me^1 in **2a**, CH_2 and Me in **3a**). The comparison shows that both the signs and values of the NMR resonances can be calculated accurately in the case of the quaternary carbons and the

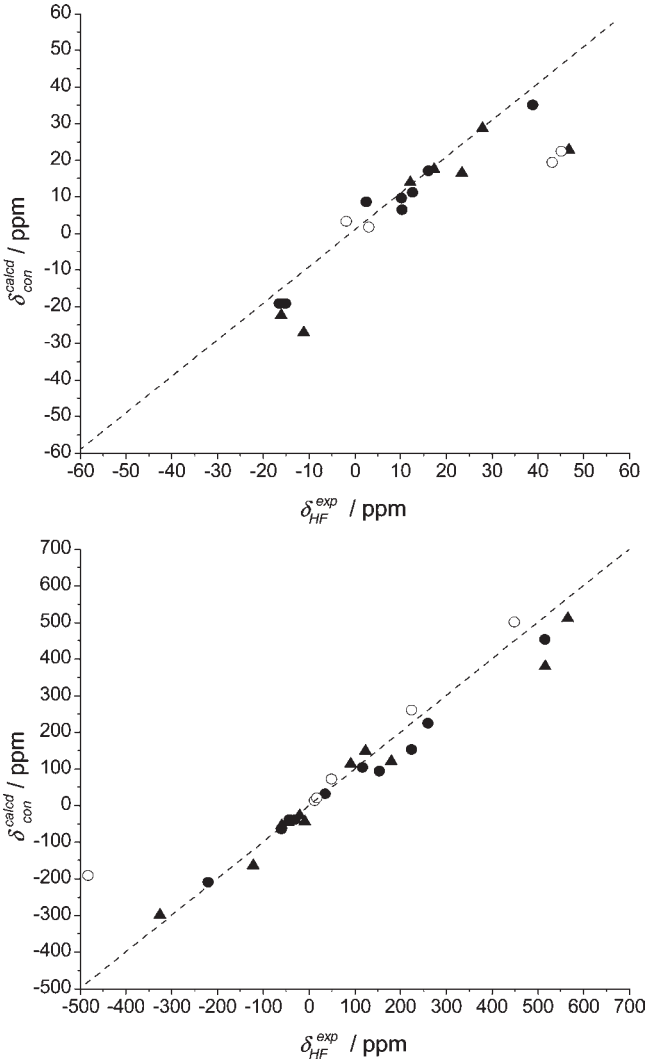

Figure 10. Comparison between calculated (Fermi contact) and experimentally derived paramagnetic ^{1}H NMR (top) and ^{13}C NMR (bottom) chemical shifts (dark circles represent **1a** data; dark triangles represent **2a** data; and open circles represent **3a** data). Dotted lines show the expected correlation.

aromatic CH groups. In the case of ^{13}C NMR, the largest deviation is registered for C^{q2} in **3a** ($\delta_{HF,T}^{exp}$ = −483.6 ppm, δ_{con}^{calcd} = −191.5 ppm). For this atom, the Fermi contact cannot be considered as the dominant factor in eq 2 any longer, and the additional terms must be taken into account. The main contribution responsible for this strong deviation is likely to be the considerable dipolar shift at C^{q2}, which is the carbon atom closest to the Ni(II) atom [d(Ni−C^{q2}) = 284.5 pm]. All other carbon atoms are much further away, so that the dipolar contribution to the hyperfine shift becomes less important.

5. Dynamic Processes

All complexes described in this study show fluxional behavior in the NMR spectra. The dynamic processes of diamagnetic complexes of bridged bisguanidines recently have been described by us.[30] Two exchanges can be observed with different exchange rates. At low temperatures, Me^1 exchanges with Me^4, and Me^2 exchanges with Me^3, respectively (see Figure 11). With a series of complexes

of the ligand btmgn (e.g., the Zn complex **2c**), we were able to show that this exchange comes not from a rotation of the C−N double bond but from an oscillation of the metal center above and below the plane defined by the ligand backbone. At higher temperatures, rotation around the C−N single bonds occurs, which leads to an exchange of the methyl groups Me^1 with Me^2 and Me^3 with Me^4, respectively.

We are now interested in applying dynamic NMR to paramagnetic compounds; therefore, we have studied the fluxional processes of the Ni complex **2a**, which has similar structural parameters, compared to the previously studied Zn complex **2c**. Two main differences between dynamic NMR of diamagnetic and paramagnetic compounds must be taken into consideration:

(a) The paramagnetic shift itself is temperature-dependent. This dependence usually obeys the Curie law, so that the resonance frequencies at slightly modified temperatures can be predicted with sufficient accuracy. In addition to that, the line shape of the paramagnetic signals changes with temperature.
(b) The signal separation in NMR spectra of chemically exchanging groups is usually much larger in paramagnetic compounds, compared to diamagnetic analogues. Consequently, faster dynamic processes are observable with paramagnetic compounds.[40]

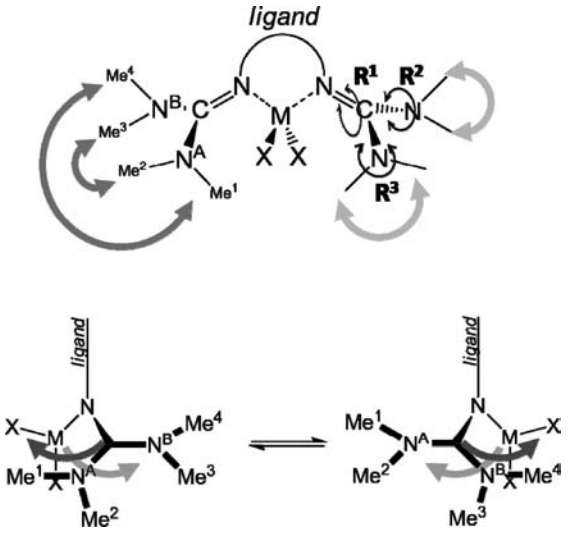

Figure 11. (Top) Dark gray arrows show the observed exchange interaction at low temperatures, light gray arrows the exchange of the methyl protons at higher temperatures. (Bottom) Side view of the molecule: an intramolecular oscillation mechanism causes the observed exchange interaction.

For these reasons, dynamic paramagnetic NMR could give insight to relatively fast dynamic processes in solution. As a proof of principle, we therefore analyzed the dynamic processes of **2a** with the aid of a line shape analysis tool.[41] We simulated not only the exchange due to the fluxional process, but also the line widths and temperature dependence of the paramagnetic shift within a single set of simulation parameters. This is possible as the paramagnetic shift results from averaging two resonances weighted by the different populations of the two sites. Because of the temperature dependence of the population difference, the chemical shift of the resulting averaged signal is, itself, temperature-dependent. Consequently, every single paramagnetic signal could be obtained by applying a fast exchange (at a rate of 10^9 s^{-1}) between a pair of signals of unequal abundance. This pair corresponds to the doublet obtained by hyperfine coupling with an unpaired electron. The NMR signal with the largest hyperfine shift (64.4 ppm at −40 °C) was simulated by two fast exchanging signals, which were arbitrarily set to +1002 and −998 ppm. With a high exchange rate and equal abundance, these two signals would lead to the diamagnetic shift of the $N-CH_3$ group at 2 ppm. By introducing an unequal abundance of the two corresponding resonances, the averaged signal is then shifted to the more-abundant signal. We then

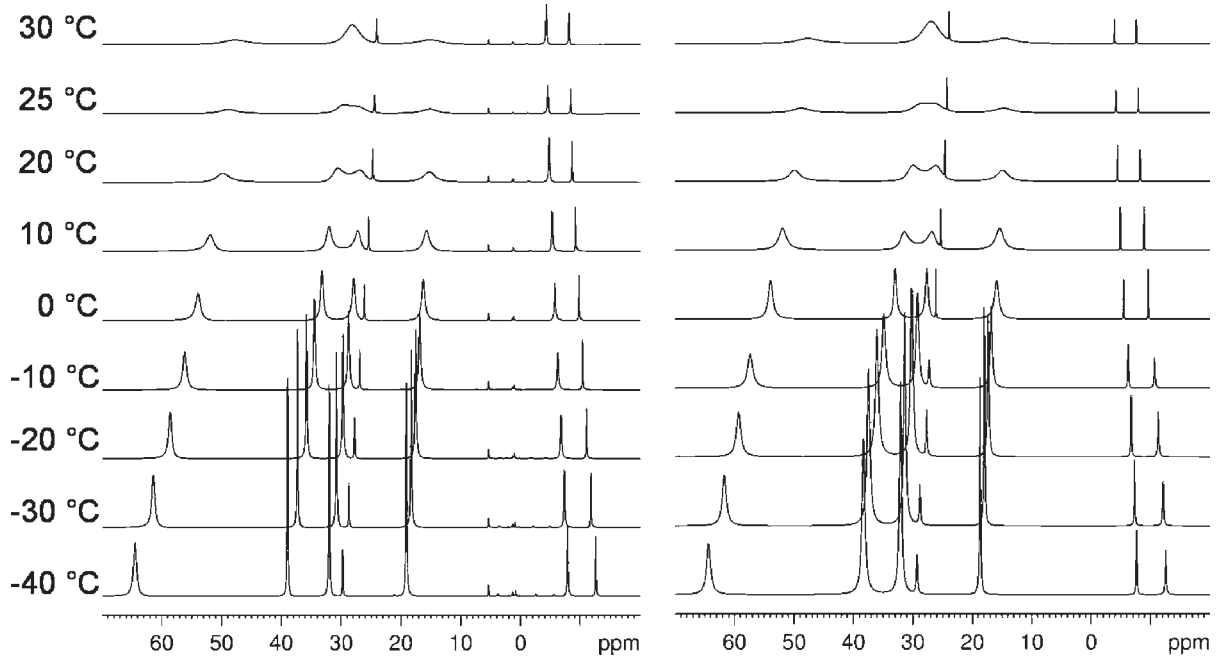

Figure 12. Experimental dynamic paramagnetic ^1H NMR spectra for **2a** (left) and simulated NMR spectra (right).

Table 4. Parameters for Paramagnetic Dynamic Line Shape Analysis of **2a**[a]

δ^{exp} (−40 °C)	δ_{orb}[b]	assignment	arbitrary ^{1}H signal splitting due to hyperfine interaction[c]
64.4	2	Me^1	2000
38.9	2	Me^3	1188
32.0	2	Me^2	984
29.7	7.5	H^β	715
19.1	2	Me^4	536
−7.9	7.5	H^α	−495
−12.6	7.5	H^γ	−655

[a] Parameters in this table were kept constant for all temperatures of the line shape analysis of **2a**. [b] Approximated value. [c] For the signal with the largest hyperfine shift (64.4 ppm at −40 °C), the signal separation due to electron−^{1}H coupling was arbitrarily set to 2000 ppm. This resulted in a population difference of 46.88:53.12 (at −40 °C). All other signal splittings were calculated for a constant population difference.

fitted the abundance for the electron Zeemann level to 46.88:53.12, so that the experimental chemical shift is reproduced.[42] Because the electron Zeemann population is valid for all NMR resonances at a specific temperature, we have then fitted all other paramagnetic signals by applying the same population difference. For the simulation of the spectra at different temperatures, only the Zeemann level population had to be modified. By this method, the experimental temperature dependence of the paramagnetic NMR shifts is reproduced well (see Figure 12 and Tables 4 and 5).

The result of the line shape analysis is shown in Table 5. The obtained exchange rates lead to an Eyring plot, as shown in Figure 13. Both activation enthalpy and activation entropy are quite similar to the preliminarily reported values of the diamagnetic analogue **2c** ($\Delta G^{\#} = 43$ kJ mol^{-1}, $\Delta S^{\#} = -41$ J mol^{-1} K^{-1}).

6. Conclusion

This work represents a detailed analysis on the use of nuclear magnetic resonance (NMR) spectroscopy to evaluate the dynamics of paramagnetic transition metal complexes. A series of paramagnetic Ni(II) halide complexes was studied, and a complete signal assignment was achieved for all complexes. The comparison of the NMR spectra recorded for Ni(II) chloride and bromide complexes and for complexes with different N−Ni−N bite angles demonstrates the sensitivity of the resonances to changes in the electron spin distribution. Experimental spin densities were derived with the help of the NMR spectra for analogous diamagnetic Zn complexes and compared with values calculated with quantum chemical (density functional theory, DFT) methods. Although the general level of agreement is satisfactory, some deviations were noted. The accumulated experimental results provide ideal calibration data for future theoretical studies. An important aspect of this work is the analysis of dynamic effects. For a typical fast process occurring in the complexes—namely, the movement of the Ni atom from one side to the other side of the aromatic guanidine ligand backbone—the rate constants were estimated from the temperature dependency of the paramagnetic shifts and a line shape analysis. The rate constants turned out to be of the same order as those for the corresponding diamagnetic Zn complexes. However, because of the signal dispersion, as a consequence of the paramagnetism, the coalescence temperature for this process is reached at a temperature that is ca. 40 °C higher than that of the corresponding diamagnetic Zn complexes. This result illustrates the possibility of using NMR studies for the detection of fast dynamic processes in paramagnetic compounds that are too fast for observation in diamagnetic NMR spectroscopy.

(40) As an example, signal coalescence at a temperature of 300 K with signal separation of 1 ppm (600 Hz at 600 MHz) corresponds to an exchange rate $k_c = 1332$ s^{-1}, whereas, for a paramagnetic example, a signal separation of 50 ppm (30 000 Hz at 600 MHz) corresponds to a rate $k_c = 66\,000$ s^{-1}.

(41) DNMR Lineshape Analysis program as part of Topspin 2.1 NMR software package (Bruker Biospin, 2009). A modified version provided by J. Rohonczy, Eötvös Loràn University, Hungary, was used.

(42) The Zeemann level populations that were used do not correspond to the real populations, because, for technical reasons, the hyperfine splitting of the reference signal Me^1 was arbitrarily set to 2000 ppm.

Table 5. Rate Constants for Chemical Exchange in **2a**, as a Result of Line Shape Analysis[a]

temperature (°C)	k [s^{-1}]	arbitrary population difference of e$^-$ Zeemann levels[b]
+30	3000	47.70:52.30
+25	2100	47.65:52.35
+20	1500	47.60:52.40
+10	1000	47.50:52.50
0	500	47.40:52.60
−10	200	47.30:52.70
−20	100	47.13:52.87
−30	50	47.01:52.99
−40	20	46.88:53.12

[a] Electron relaxation was set to 10^9 s^{-1}. [b] Population difference as result of arbitrary electron−^{1}H coupling (see Table 4 and ref 42).

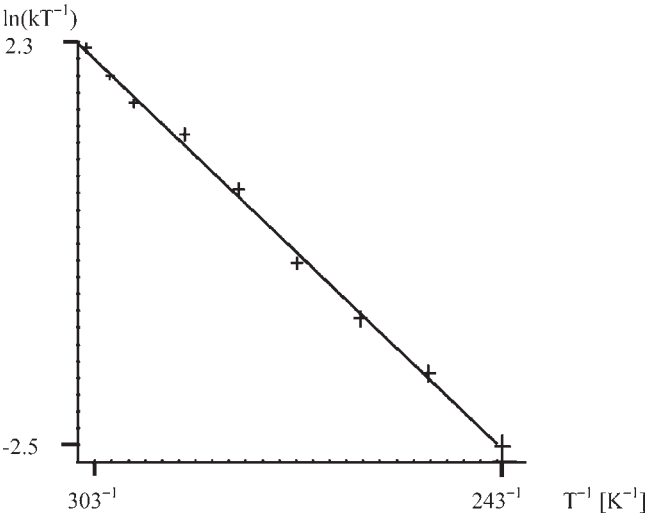

Figure 13. Eyring plot as result of the line shape analysis of **2a**. $\Delta G^{\#} = 39.6 \pm 2$ kJ mol^{-1}, $\Delta S^{\#} = -48 \pm 15$ J mol^{-1} K^{-1}.

7. Experimental and Computational Details

All Ni complexes were prepared and worked up as described previously,[29,31] by applying standard Schlenk techniques, and handled under a strict argon atmosphere. Acetonitrile was purchased by Aldrich, stored under an inert argon atmosphere, and subjected to a 3 Å molecular sieve. Toluene was dried with standard techniques, stored under an inert argon atmosphere, and also subjected to a 4 Å molecular sieve. All reagents were purchased from Acros Organics and used without any further purification.

Experimental Section. 1c. A quantity of 125.5 mg (0.33 mmol) of btmgbp are dissolved in 10 mL CH_3CN, and 0.3 mL of a 1 M

$ZnCl_2$ solution in Et_2O is added dropwise. The reaction mixture is then stirred for a period of 24 h at room temperature. Subsequently, the solvent is removed under vacuum and the residue washed three times with 5 mL of toluene, to clean the product from unreacted btmgbp. After the removal of all solvent traces under vacuum, 141.1 mg (0.273 mmol, 91%) of **1c** are obtained as a white powder. Recrystallization from CH_3CN at −21 °C affords colorless crystals suitable for X-ray diffraction (XRD) study. $C_{22}H_{32}Cl_2N_6Zn$ (516.83): calcd. C 51.12, H 6.24, N 16.26, Cl 13.72, Zn 12.66; found C 51.40, H 6.37, N 16.08. ^{1}H NMR (600.13 MHz, CD_2Cl_2, 22 °C): δ = 7.30 (t, 2H, CH_{arom}), 7.15 (t, 2H, CH_{arom}), 7.04 (d, 2H, CH_{arom}), 6.58 (d, 2H, CH_{arom}), 3.37 (s, 6H, CH_3), 2.78 (s, 6H, CH_3), 2.64 (s, 6H, CH_3), 2.04 (s, 6H, CH_3) ppm. ^{13}C NMR (100.55 MHz, CD_2Cl_2, 22 °C): δ = 166.41 (CN_3), 148.52 ($C_{q,arom}$), 137.03 ($C_{q,arom}$), 133.61 ($C_{q,arom}$), 129.46 (CH_{arom}), 125.50 (CH_{arom}), 124.47 (CH_{arom}), 42.40 (CH_3), 41.57 (CH_3), 40.59 (CH_3), 39.31 (CH_3) ppm. IR (KBr, cm^{-1}): ν = 3058(w), 3012(w), 2932(m), 2885(m), 2799(w), 1530(vs), 1467(s), 1417(s), 1333(m), 1272(w), 1242(m), 1203(w), 1157(m), 1104(w), 1036(w), 1002(w), 935(w), 863(m), 813(m), 753(m), 697(w), 626(w), 576(w), 522(m). HR-EI$^+$: Calc, m/z = 516.1346 [$C_{22}H_{32}N_6Cl_2Zn$]; exp, m/z = 516.1362 $[M]^+$. FAB$^+$: m/z = 516.1 $[M]^+$, 478.2 $[M-Cl]^+$, 380.3 $[btmgbp]^+$. Crystal data for **1c**·CH_3CN, $C_{24}H_{35}Cl_2N_7Zn$: M_r = 557.86, 0.40 mm × 0.30 mm × 0.30 mm, monoclinic, space group $P2(1)/n$, a = 15.586(3) Å, b = 9.788(2) Å, c = 18.326(4) Å, β = 98.87(3)°, V = 2762.3(10) Å^3, Z = 4, d_{calc} = 1.341 Mg m^{-3}, Mo $K\alpha$ radiation (graphite-monochromated, λ = 0.71073 Å), T = 100 K, θ_{range} = 1.60°−33.05°. Reflections: measd. 95957, indep. 8074. R_{int} = 0.0507. Final R indices [$I > 2\sigma(I)$]: R_1 = 0.0431, wR_2 = 0.1082.

3c. A quantity of 148.0 mg (0.49 mmol) bdmegb are dissolved in 10 mL of CH_3CN, and 0.4 mL of a 1 M $ZnCl_2$ solution in Et_2O is added dropwise. The reaction mixture is then stirred for a period of 24 h at room temperature. Subsequently, the solvent is removed under vacuum and the residue washed three times with 5 mL of toluene to clean the product from traces of unreacted bdmegb. After drying under vacuum, 160.7 mg (0.368 mmol, 92%) of **3c** are obtained as a white powder. Recrystallization from CH_3CN at −21 °C affords colorless crystals suitable for XRD study. $C_{16}H_{24}Cl_2N_6Zn$ (436.72): calcd. C 44.00, H 5.54, N 19.24, Cl 16.24, Zn 14.98; found C 44.10, H 5.58, N 19.07. ^{1}H NMR (399.89 MHz, CD_2Cl_2, 22 °C): δ = 6.81 (m, 4H, CH_{arom}), 3.58 (m, 8H, CH_2), 2.85 (m, 6H, CH_3) ppm. ^{13}C NMR (100.55 MHz, CD_2Cl_2, 22 °C): δ = 163.75 (CN_3), 139.30 ($C_{q,arom}$), 121.87 (CH_{arom}), 121.24 (CH_{arom}), 49.12 (CH_2), 36.21 (CH_3) ppm. IR (KBr, cm^{-1}): ν = 3052(w), 2932(m), 2881(m), 2805(w), 1599(s), 1563(vs), 1481(s), 1412(s), 1392(s), 1289(s), 1237(m), 1105(w), 1087(w), 1035(m), 980(w), 855(w), 811(m), 764(m), 741(m), 702(w), 650(w), 603(w), 555(w). HR-FAB$^+$: calc, m/z = 436.0695 [$C_{16}H_{24}N_6Cl_2Zn$]; exp, m/z = 436.0699 $[M]^+$. FAB$^+$: m/z = 436.2 $[M]^+$, 399.2 $[M-Cl]^+$, 300.3 $[bdmegb]^+$. Crystal data for **3c**·CH_3CN: M_r = 477.74, 0.40 mm × 0.40 mm × 0.35 mm, monoclinic, space group $P2(1)$, a = 8.7900(18) Å, b = 10.346(2) Å, c = 12.569(3) Å, β = 106.43(3)°, V = 1096.4(4) Å^3, Z = 2, d_{calc} = 1.447 Mg m^{-3}, Mo $K\alpha$ radiation (graphite-monochromated, λ = 0.71073 Å), T = 100 K, θ_{range} = 1.69°−33.19°. Reflections: measd. 25847, indep. 7832. R_{int} = 0.0476. Final R indices [$I > 2\sigma(I)$]: R_1 = 0.0328, wR_2 = 0.0726.

NMR Measurements. The complexes were dissolved in deuterated dichloromethane, which was stored under an inert argon atmosphere and subjected to a 4 Å molecular sieve. ^{1}H NMR spectra were referenced to the residual protio signal of the solvent (δ = 5.31 ppm) and ^{13}C NMR spectra to the solvent triplet at δ = 53.80 ppm. The samples were prepared in NMR tubes that were flame-sealed afterward. The variable-temperature ^{1}H NMR studies and relaxation time determination T_1 were accomplished on a Bruker Model DPX-200 that was equipped with a BVT3300 temperature unit. The temperatures were calibrated using samples of glycol (pure, temperature range of 300−380 K) or methanol (pure, 180−300 K), respectively. ^{1}H NMR as well as all ^{13}C NMR experiments were carried out on a Bruker AVANCE III 600 system that was equipped with a cryogenically cooled detection probe (QNP Cryo-Probe). Typical parameters for ^{13}C NMR spectra: repetition rates, 0.1−0.3 s; pulse widths, 3−6 μs (corresponding to pulse angles of 30°−60°); 0.01−0.1 s; number of scans, 1000−30000; exponential multiplication with a line-broadening factor of 10−30 Hz. Measurements of the relaxation time T_1 were done using the inversion recovery method.

X-ray Crystallographic Studies. Suitable crystals were taken directly from the mother liquor, immersed in perfluorinated polyether oil, and fixed on top of a glass capillary. Measurements were made on a Nonius−Kappa CCD diffractometer with a low-temperature unit, using graphite-monochromated Mo Kα radiation. The temperature was set to 100 K. The data collected were processed using the standard Nonius software.[43] All calculations were performed using the SHELXT-PLUS software package. Structures were solved by direct methods with the SHELXS-97 program and refined with the SHELXL-97 program.[44,45] Graphical handling of the structural data during solution and refinement was performed with XPMA.[46] Atomic coordinates and anisotropic thermal parameters of non-hydrogen atoms were refined by full-matrix least-squares calculations. Crystallographic data (excluding structure factors) for the structures reported in this paper have been deposited with the Cambridge Crystallographic Data Centre, as supplementary publications No. CCDC 769711 and No. CCDC 769712. Copies of the data can be obtained free of charge upon application to the CCDC, 12 Union Road, Cambridge CB2 1EZ, U.K. [Fax: (international) +44 (0)1223/336033; E-mail: deposit@ccdc.cam.ac.uk.]

Calculational Details. All optimization and spin density calculations were carried out using the Gaussian 03[47] program package. The B3LYP[48] functional, in combination with a set of two different basis sets, was used: For the Ni atom, a Karlsruhe triple-ζ quality basis set of the second generation with a larger set of polarization functions was used (Def2-TZVPP),[49] whereas the C, N, halide, and H atoms were described by the 6-311G(d,p) basis set.[50] This combination will be labeled as BS-I throughout

(43) DENZO-SMN, Data processing software; Nonius, 1998 (ttp://www.nonius.com).

(44) (a) Sheldrick, G. M. *SHELXS-97, Program for Crystal Structure Solution*; University of Göttingen, 1997 (http://shelx.uni-ac.gwdg.de/SHELX/index.html). (b) Sheldrick, G. M. *SHELXL-97, Program for Crystal Structure Refinement*; University of Göttingen, 1997 (http://shelx.uni-ac.gwdg.de/SHELX/index.html).

(45) *International Tables for X-ray Crystallography*, Vol. *4*; Kynoch Press: Birmingham, U.K., 1974.

(46) Zsolnai, L.; Huttner, G. *XPMA*; University of Heidelberg, 1994 (http://www.uni-heidelberg.de/institute/fak12/AC/huttner/software/software.html).

(47) Frisch, M. J.; Trucks, G. W.; Schlegel, H. B.; Scuseria, G. E.; Robb, M. A.; Cheeseman, J. R.; Montgomery, J. A. Jr.; Vreven, T.; Kudin, K. N.; Burant, J. C.; Millam, J. M.; Iyengar, S. S.; Tomasi, J.; Barone, V.; Mennucci, B.; Cossi, M.; Scalmani, G.; Rega, N.; Petersson, G. A.; Nakatsuji, H.; Hada, M.; Ehara, M.; Toyota, K.; Fukuda, R.; Hasegawa, J.; Ishida, M.; Nakajima, T.; Honda, Y.; Kitao, O.; Nakai, H.; Klene, M.; Li, X.; Knox, J. E.; Hratchian, H. P.; Cross, J. B.; Bakken, V.; Adamo, C.; Jaramillo, J.; Gomperts, R.; Stratmann, R. E.; Yazyev, O.; Austin, A. J.; Cammi, R.; Pomelli, C.; Ochterski, J. W.; Ayala, P. Y.; Morokuma, K.; Voth, G. A.; Salvador, P.; Dannenberg, J. J.; Zakrzewski, V. G.; Dapprich, S.; Daniels, A. D.; Strain, M. C.; Farkas, O.; Malick, D. K.; Rabuck, A. D.; Raghavachari, K.; Foresman, J. B.; Ortiz, J. V.; Cui, Q.; Baboul, A. G.; Clifford, S.; Cioslowski, J.; Stefanov, B. B.; Liu, G.; Liashenko, A.; Piskorz, P.; Komaromi, I.; Martin, R. L.; Fox, D. J.; Keith, T.; Al-Laham, M. A.; Peng, C. Y.; Nanayakkara, A.; Challacombe, M.; Gill, P. M. W.; Johnson, B.; Chen, W.; Wong, M. W.; Gonzalez, C.; Pople, J. A. *Gaussian 03, Revision E.01*; Gaussian, Inc.: Wallingford, CT, 2004.

(48) (a) Becke, A. D. *J. Chem. Phys.* **1993**, *98*, 5648–5652. (b) Lee, C.; Yang, W.; Parr, R. G. *Phys. Rev. B* **1988**, *37*, 785–789.

(49) Weigend, F.; Ahlrichs, R. *Phys. Chem. Chem. Phys.* **2005**, *7*, 3297–3305.

this paper. It should be emphasized that the 6-311G(d,p) basis set used for the ligand atoms is of lower quality than the TZVPP basis set used for Ni. Nevertheless, the combination was applied because of computational restrictions.

Acknowledgment. The authors gratefully acknowledge financial support from the Deutsche Forschungsgemeinschaft, especially through the Graduate College 850 and the priority program SPP 1178. We thank Dr. J. Rohonczy (Eötvös Loránd University, Hungary) for providing a modified version of the DNMR program.

Supporting Information Available: This material is available free of charge via the Internet at http://pubs.acs.org.